Effect of mixed salts on atmospheric corrosion of 304 stainless steel

Guo, Liya; Mi, Na; Haval B., Mohammed-Ali; Majid, Ghahari; Du Plessis, Andrew; Cook, Angus; Street, Steven; Reinhard, C.; Atwood, Robert C; Rayment, Trevor; Davenport, Alison

DOI:
10.1149/2.0021911jes

JES Focus Issue on Electrochemical Techniques in Corrosion Science in Memory of Hugh Isaacs

Effect of Mixed Salts on Atmospheric Corrosion of 304 Stainless Steel

Liya Guo,[1,2,z] Na Mi,[1] Haval Mohammed-Ali,[1,3] Majid Ghahari,[1] Andrew Du Plessis,[1] Angus Cook,[1] Steven Street,[1] Christina Reinhard,[4] Robert C. Atwood,[4] Trevor Rayment,[4] and Alison J. Davenport[1,*,z]

[1] *School of Metallurgy and Materials, University of Birmingham, West Midlands B15 2TT, United Kingdom*
[2] *Department of Materials, Imperial College London, London SW7 2AZ, United Kingdom*
[3] *Physics Department, University of Zakho, Zakho, Iraq*
[4] *Diamond Light Source Ltd., Oxfordshire OX11 0DE, United Kingdom*

Atmospheric corrosion of stainless steel can take place when airborne salt particles deposit on the metal surface, forming droplets when the relative humidity (RH) reaches a critical value: the deliquescence relative humidity of the salt. Most work to date has focused on single salts such as $MgCl_2$ or NaCl. In the present work, the effect of mixed salts is investigated at 45% RH, above the deliquescence relative humidity of $MgCl_2$ but below that of NaCl. Dish-shaped pits were found in pure $MgCl_2$ solutions and mixed solutions. Crevice corrosion takes place under NaCl crystals. This is shown both with ex situ measurements and in situ time-dependent measurements using X-ray microtomography, where pit growth was also monitored.
 [DOI: 10.1149/2.0021911jes]

Manuscript submitted September 26, 2018; revised manuscript received December 28, 2018. Published January 9, 2019. *This paper is part of the JES Focus Issue on Electrochemical Techniques in Corrosion Science in Memory of Hugh Isaacs.*

In marine environments, airborne sea salt particles (salt aerosols) can be deposited on stainless steel surface by coastal winds.[1] Salt will absorb moisture from the environment when its deliquescence relative humidity (DRH) is below the relative humidity (RH) of the surrounding environment until the vapor pressure of the solution reaches that of the environment. If the solution is aggressive enough, particularly in the presence of chloride ions, localized corrosion can start. The degree of deliquescence varies with salt composition since salts have specific DRH values. For example, the DRH of the two major constituents of sea water, NaCl and $MgCl_2$, are 75% and 33%, respectively.[2]

The composition of deposited aerosols varies with the studied area.[1,3,4] However, most work on chloride salts to date has focused either on single salts such as $MgCl_2$[5–8] and NaCl,[9–11] or artificial sea water.[5,12] For 304 and 403 stainless steel, pitting was more likely to take place under artificial sea water than $MgCl_2$ droplets.[5,12] There is a need to study the effect of mixed salts with different compositions on stainless steel. This work focuses on a mixture of NaCl and $MgCl_2$ as these are two major components of artificial sea water.[13]

It is difficult to observe pit propagation with time since the growth takes place under droplets that develop rust layers. However, in situ synchrotron X-ray microtomography makes it possible to visualize the growth of pits in a non-destructive way. This method has been used in recent years to study in situ corrosion processes.[14–21]

In the present work, the effect of mixed salts is investigated at an RH above the DRH of $MgCl_2$ but below that of NaCl. For ex situ lab-based tests, characterization was carried out at the end of the test whereas for synchrotron X-ray microtomography tests, in situ characterization was performed at several points during the exposure period.

Experimental

Material.—For lab-based tests, 304 stainless steel foils (annealed, 100 μm in thickness, supplied by Goodfellow) were cut into 3 cm × 6 cm. For synchrotron microtomography tests, 304 stainless steel pin samples (2 mm in diameter) were cut from a rod (drawn, 2 mm in diameter, supplied by Goodfellow). The composition of the 304 foil and pin is 17–20 wt% Cr, 8–11 wt% Ni, <2 wt% Mn, <800 ppm C and Fe balance.

Droplet deposition.—The foil and pin samples were ground with SiC papers to P800 and washed with de-ionized water (Millipore > 15 MΩ.cm) and methanol. 0.5 M $MgCl_2$ and 0.25 M $MgCl_2$+ 0.5 M NaCl (1$MgCl_2$:2NaCl) were used for droplet deposition. A droplet, containing 1.8 μL of solution, was deposited onto the foil/pin surface. In lab-based tests, the droplet diameter was 2.2–2.8mm, giving a chloride deposition density (CDD) of 900 to 1600 μg/cm^2. In tomography tests, the droplet diameter was 2 mm, giving a CDD of 2000 μg/cm^2.

Relative humidity and temperature.—In lab-based tests, after deposition of droplets, foils were put into a transparent desiccator. The 45% exposure RH was controlled by 4.25 M $MgCl_2$[5] or saturated K_2CO_3.[2] The 21°C test temperature was controlled by an atmospheric chamber. OMEGA OM-EL-USB-2-LCD data loggers were used to monitor the RH and temperature during the corrosion test. In tomography tests, filter paper soaked with 4.25 M was fitted into a silicone tube, which were slipped over the pin. Tomography tests were carried out at 21 ± 1°C.

Ex situ lab-based corrosion tests.—For lab-based experiments, the corrosion behavior of 304 foils under $MgCl_2$ after 48 h exposure time and under mixed salts $MgCl_2$ + NaCl after 24 h, 48 h and 72 h exposure time was investigated. After exposure tests, a Leica DFC 420 light optical microscope (OM) was used to characterize the pit size. The width of a pit refers to the diameter of a circle which has the same area as the pit area. The depth of a pit is defined as the greatest depth found among different parts of a pit. Pit depths were measured by OM by using the depth of focus.

In situ synchrotron X-ray microtomography tests.—The design of the cell for in situ X-ray microtomography studies has been detailed previously.[22] Samples were scanned regularly to examine the time-dependent pit growth. The tomography experiments using 70 keV X-rays were performed on the Beamline I12[23] at Diamond Light Source. The pin was rotated and radiographs were collected at intervals 0.1° per step through 180°. During scanning, two exposure times were used: 1.0 s exposure time was used with a pixel size of 1.8 μm, and 2.2 s exposure time was used with a pixel size of 0.9 μm.

*Electrochemical Society Member.
[z]E-mail: liya.guo@imperial.ac.uk; a.davenport@bham.ac.uk

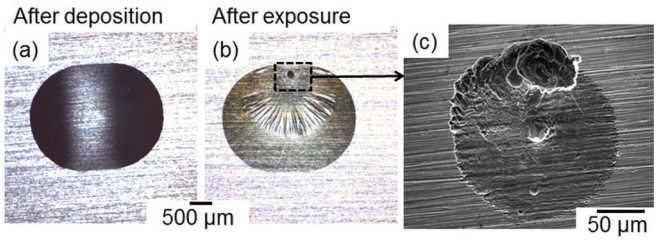

Figure 1. OM images of 304 foil with a $MgCl_2$ droplet with a CDD of 1110 µg/cm^2 (a) after deposition and (b) after exposure at 45 ± 2% RH and 21 ± 1°C for 48 h. A pit under the droplet was highlighted by a dashed square and also shown with (c) an SEM image.

The total scanning time per sample was ~40 minutes for the lower magnification scans and ~80 minutes for the high magnification scans. Filtered back-projection was used during reconstruction. Fiji[24] was used for 2D visualization and characterization of the pit, and Avizo software was used for 3D characterization of the pit.[25] In tomography, the top surface area of the pit is defined as the pit area. The width of a pit refers to the diameter of a circle which has the same area as the pit area. Pit depth was measured from the pit mouth to the pit bottom.

Results and Discussion

Localized corrosion under $MgCl_2$.—Figure 1 shows a typical droplet after deposition (Figure 1a) and exposure at 45 ± 2% RH and 21°C for 48 h (Figure 1b) in a lab-based experiment. The droplet after deposition was not perfectly circular and showed elongation along the grinding direction. After exposure, a single pit and rust can be observed under the droplet (Figure 1b). The surface of the droplet appears to have a wrinkled skin. The nature of the skin is not known as it is difficult to isolate. Following removal of the droplet and corrosion products, the pit was further examined in SEM and shown in Figure 1c. 20 out of 23 droplets showed pitting corrosion after exposure. Only one pit was found under each droplet. Figure 1c shows a pit with "spiral" growth, consistent with growth under cathodically-limited conditions.[6,8] When the pit width is calculated, both the shallow and the deep part are taken into account.

Localized corrosion under mixed salt: $MgCl_2$ + NaCl.—Under mixed salt droplets containing $MgCl_2$ + NaCl, crystals form as the RH is reduced to 45% RH as shown in Figure 2a. The process where water evaporates from the salt solution is called efflorescence. The crystals are likely to be NaCl particles, given that the RH is in the range of the reported efflorescence relative humidity (ERH) of NaCl, which is 41% to 51% RH.[26–31] $MgCl_2$ is expected to remain in solution since the DRH of $MgCl_2$ (33%) is lower than the exposure RH. Therefore, solution layers can also be observed.

Figure 2b shows the vertical section of an X-ray tomogram of a pin sample, deposited with a 1$MgCl_2$:2NaCl droplet, after exposure at 45 ± 2% RH and 21 ± 1°C for 17 h. It clearly shows the presence of crystals on top of the pin sample.

In lab-based experiments, mixed salt droplets were deposited onto 304 foils and exposed at 45 ± 2% RH and 21°C for 24 h, 48 h and 72 h. 18 droplets were studied for 24 h or 72 h exposure time. 41 droplets were studied for 48 h exposure time. After exposure, all droplets showed pitting between or under crystals, or crevice corrosion under crystals.

Figure 3 shows three typical forms of corrosion attack found under droplets after exposure. Figures 3a–3c show micrographs of selected regions of the three droplets after exposure for 48 h. Figures 3d–3f show the foil surfaces of the same droplets following washing with deionized water at the end of the test. Figures 3g–3i are SEM images that show the corrosion morphology of the same samples, illustrating the three typical types of corrosion behavior: a dish-shaped pit between

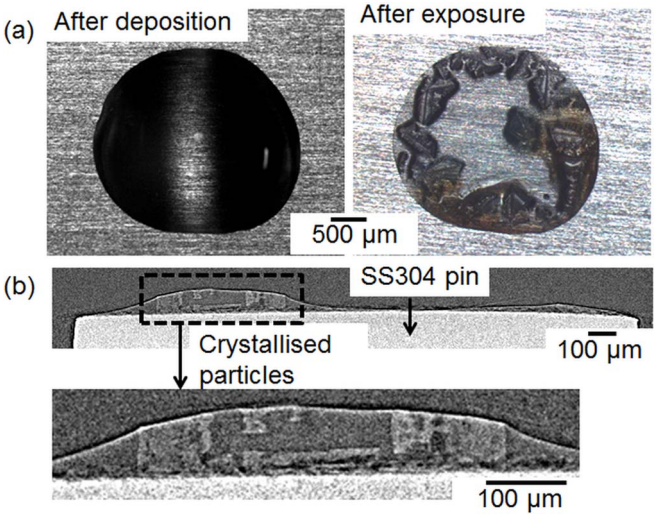

Figure 2. (a) Optical microscope images of 304 foils under a 1$MgCl_2$:2NaCl mixed salt droplet with a CDD of 1140 µg/cm^2 after deposition and after exposure at 45 ± 2% RH and 21°C for 48 h. (b) Vertical sections of an X-ray tomogram of a 304 pin under a 1$MgCl_2$:2NaCl mixed salt droplet with a CDD of 2000 µg/cm^2 after exposure at 45 ± 2% RH and 21 ± 1°C for 17 h. A higher magnification view of the crystal is shown in (b).

crystals, shallow crevice-like attack under a crystal, and crevice-like attack containing a pit under a crystal.

Figures 3a, 3d and 3g show a pit found between crystals. It is dish-shaped and is ~100 µm in width and ~50 µm in depth. The morphology of the pit is similar to the deep region of the pit in Figure 1. However, there is no indication of the large shallow region that is generally observed to develop initially during pit growth in $MgCl_2$.[8] The reason for this is not clear.

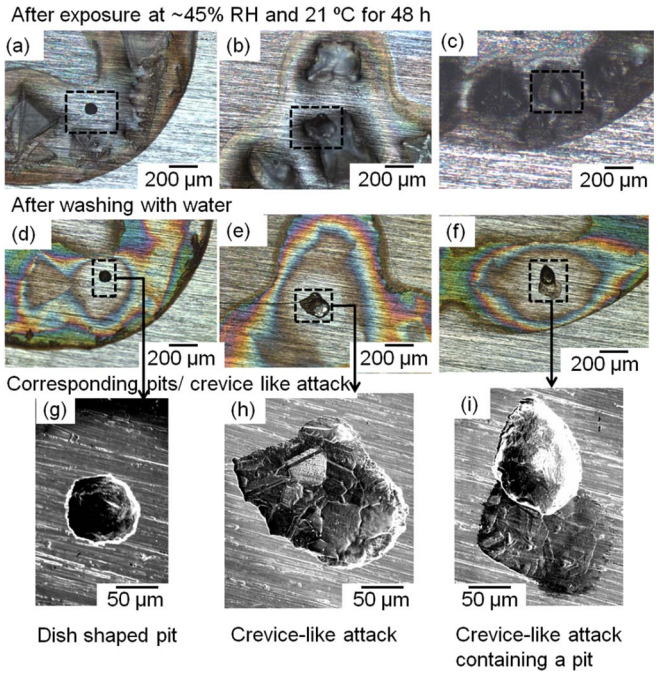

Figure 3. (a)-(f): Optical microscope images of 304 foil under three 1$MgCl_2$:2NaCl mixed salt droplets (CDD varying from 1060 to 1300 µg/cm^2) (a)-(c): after exposure at 45 ± 2% RH and 21 ± 1°C for 48 h and (d)-(f) following washing with water. (g)-(i) SEM images of the pits/crevice-like attack/crevice-like attack containing a pit observed under the droplets shown in (a)-(c).

Figures 3b, 3e and 3h show a crevice under a crystal: it is wide and shallow (~200 μm in width and ~20 μm in depth). The depths of four crevice-like attack sites after exposure for 48 h are from 5 to 30 μm. Most of the crevice-like attack was irregular and showed crystallographic etching (Figure 3h). This type of corrosion attack was only found under crystals, which were regarded as crevice-formers. Crevice-like corrosion on 304L under salt crystals was also reported by Cook[32] in his study of $MgCl_2$ and $MgSO_4$ mixtures.

Figures 3c, 3f and 3i illustrate crevice-like attack containing a dish-shaped pit (~200 μm in width and ~35 μm in depth). The depths of three different sites of crevice-like attack containing dish-shaped pits (after exposure for 48 h) varied from 10 to 35 μm. It was not clear whether the crevice-like attack or the dish-shaped pit formed first. The morphology of these pits is somewhat similar to the spiral pits observed under pure $MgCl_2$. However, the crevice-like attack containing a dish-shaped pit was only found under crystals.

Pin samples under mixed salt droplets were imaged with X-ray microtomography, as shown in Figure 4. The left and right images are the horizontal and vertical sections of the tomogram, respectively.

Figure 4a shows a dish-shaped pit between crystals. Figure 4b illustrates crevice-like attack under a crystal. Compared with the dish-shaped pit shown in Figure 4a, the crevice-like attack found here is wider and shallower. Figure 4c shows crevice-like attack containing a pit under a crystal. Pitting corrosion under droplet electrolyte layers and crevice corrosion under crystals in synchrotron X-ray microtomography is consistent with that found in following lab-based experiments. However, it should be noted that multiple pits (more than four) were found on each of the pin samples in tomography experiments while the observation of single pits was most frequent in lab-based tests. The observation of multiple pits in tomography experiments might be due to the microstructure difference between the pin and foil samples. This observation might also indicate the presence of beam-induced pit initiation.[15,33,34] The interaction between an intense X-ray beam and water might produce radiolytic products, and affect the electrochemical processes.[34]

Figure 5 gives a summary of the corrosion behavior on 304 foils under mixed salt droplets after exposure for 24, 48 or 72 h in lab-based experiments. One single dish-shaped pit was most frequently observed under the experimental conditions studied here. All droplets contained at least one corrosion site (pit or crevice).

Since one single pit under a droplet after exposure was the most common observation for both $MgCl_2$ and $1MgCl_2$:2NaCl droplets, the widths and depths of these pits were studied further. Figure 6 is a summary of the widths and depths of 10 single pits, found under $MgCl_2$ droplets or $1MgCl_2$:2NaCl mixed salt droplets (under

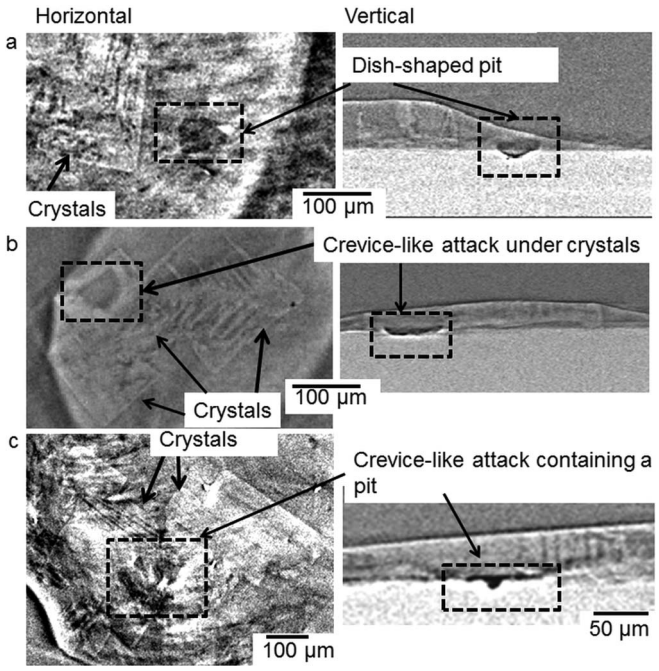

Figure 4. Observation of (a) a dish-shaped pit under solution layers (b) crevice-like attack under a NaCl crystal and (c) crevice-like attack containing a pit under a NaCl crystal found on a 304 pin sample in horizontal section above the pit/attack and vertical section through the pit/attack and solution layers under a mixed salt droplet: $1MgCl_2$:2NaCl with a CDD of 2000 μg/cm^2 after exposure at 45 ± 2% RH and 21 ± 1°C for 34 h. Dashed squares are used to highlight the pit/attack. The sample was monitored in in situ X-ray microtomography.

electrolyte layers between crystals). The overall width of pits observed under $MgCl_2$ are commonly greater than the dish-shaped pits under $1MgCl_2$:2NaCl because of the wide shallow region (Figure 1c) that forms initially in these droplets.[8] However, there is no obvious trend for pit depths.

Pits in mixed salt droplets are under electrolyte layers between crystals and therefore diffusion of ions away from the pit is expected to be decreased due to the diffusion barrier provided by the neighboring NaCl crystals. Therefore, an aggressive environment for pit initiation and propagation is more easily developed and maintained. The observation (Figure 6) that the widths of the dish-shaped pits

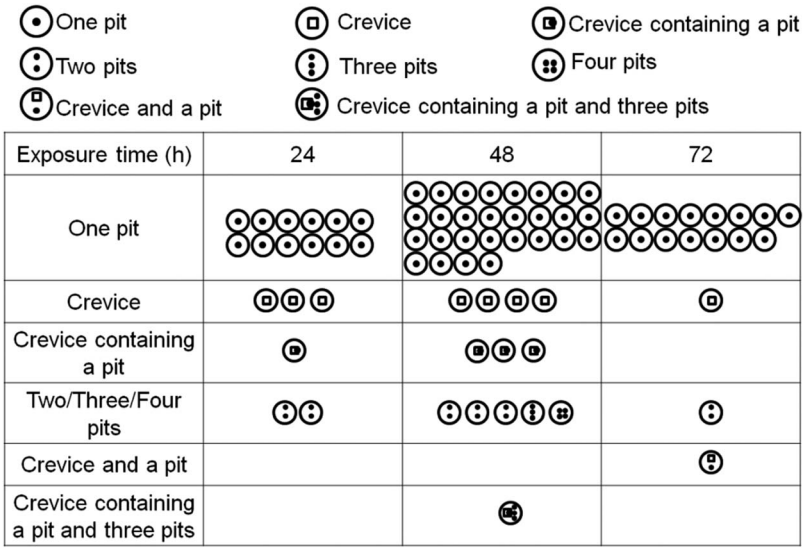

Figure 5. Summary of observations of pits or crevice-like attack found on 304 foils deposited with $1MgCl_2$:2NaCl mixed salt droplets with a CDD varying from 900 to 1600 μg/cm^2 after exposure at 45 ± 2% RH and 21 ± 1°C for 24, 48 or 72 h in lab-based tests. 18 droplets were tested for 24 h or 72 h exposure time. 41 droplets were tested for 48 h exposure. All droplets contained at least one corrosion site (pit or crevice).

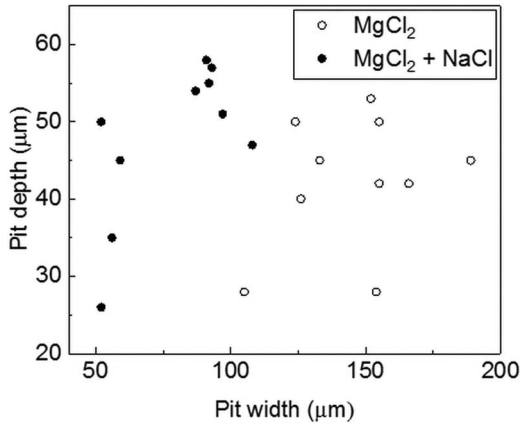

Figure 6. Depth and width of 10 pits found on 304 foil under $MgCl_2$ or $1MgCl_2$:2NaCl droplets with a CDD varying from 900 to 1600 $\mu g/cm^2$, after exposure at 45 ± 2% RH and 21°C for 48 h. Only single pits under a droplet after exposure was taken into account.

under mixed salt droplets are generally smaller than those of the spiral pits under pure $MgCl_2$ droplets might be due to the smaller surface area available for the cathodic reaction (reduction of oxygen),[35] and increased solution resistance, again provided by the crystals, which will lead to a greater IR drop between the cathodic areas and the pit. Furthermore, while the initial volume and CDD of the droplets are the same for the mixed salt and pure $MgCl_2$ droplets, precipitation of NaCl crystals will remove most of the sodium ions and nearly half of the chloride ions from the electrolyte. This will reduce the volume of the electrolyte layer by nearly half compared with that for pure $MgCl_2$ solutions since the final exposure RH, which controls the concentration of the electrolyte layers, was the same. The decreased electrolyte volume/thinner electrolyte layer also leads to a greater IR drop. Previous studies have also reported that the pit width is *IR*-controlled[8,15,36] which may provide an explanation for the observation that the widths of the pits under mixed $MgCl_2$ + NaCl were smaller than those under pure $MgCl_2$.

Pit growth with time.—Samples were examined at different exposure times: 3 h, 17 h, 34 h and 69 h or 79 h in tomography experiments. Figure 7a shows the growth of the dish-shaped pit shown in Figure 4a. There is no obvious sign of pitting after 3 h. After 17 h, a very small hole surrounded by a very shallow pit area can be observed from the vertical section. After 34 h, a dish-shaped pit was found. The pit grew between 34 h and 79 h. Figure 7b shows the pit size after exposure for 34 h and 79 h. Although there is little increase in pit width and pit depth, there is a substantial pit volume increase from ~16000 μm^3 to 26000 μm^3.

Figure 8 shows the growth of crevice-like attack under the crystal shown in Figure 4b. After exposure for 3 h, there was no obvious crevice corrosion, while crystals formed. After exposure for 17 h, crevice-like attack was found. Both the width and depth of the crevice-like attack increased during the subsequent exposure. The pit volume changed greatly from 7300 μm^3 (after exposure for 17 h) to 38000 μm^3 (after exposure for 69 h). It is seen that growth, once initiated, continued throughout the experiment. According to the data in Figure 8, the square of pit depth is nearly linear with exposure time. This dependence is consistent with the idea that pit depth is under diffusion control,[36] but could also be associated with decreasing cathodic current. However, the data are too limited to draw any broader conclusion.

Localized corrosion behavior in realistic atmospheric conditions.—The current study shows that different morphologies - dish-shaped pits and crevice-like attack - can both be observed in salt droplets in atmospheric conditions where mixed salts are present. This

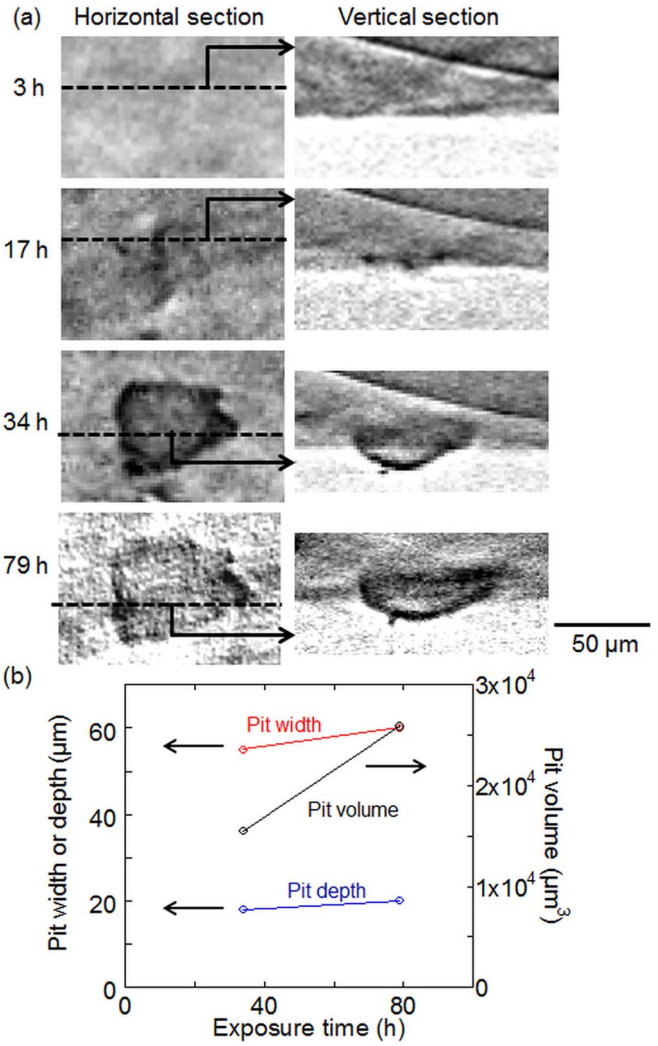

Figure 7. (a) Observation of horizontal and vertical sections of the tomogram of a dish-shaped pit (shown in Figure 4) imaged with X-ray microtomography on a 2 mm 304 pin deposited with a $1MgCl_2$:2NaCl mixed salt droplet with a CDD of 2000 $\mu g/cm^2$ following exposure at 45 ± 2% RH and 21 ± 1°C for 3 h, 17 h, 34 h and 79 h. (b) Width, depth and volume of the dish-shaped pit at 34 h and 79 h.

is a particular concern for surfaces that are under stress where there is a risk of environmentally-assisted cracking. The morphology of the pit/crevice-like attack might affect the susceptibility of the pit developing into a crack since the morphology might affect the stress/strain distribution.[37,38] This indicates the importance of studying the effect of composition variation as a function of relative humidity for conditions where mixed salts are found.

Conclusions

- Atmospheric corrosion of stainless steel has been investigated under salt droplets containing a mixture of NaCl and $MgCl_2$ at 21 ± 1°C and 45 ± 2% RH. This value is above the deliquescence relative humidity of $MgCl_2$ and in a region where the formation of solid NaCl crystals is expected.
- Ex situ lab-based tests showed three types of corrosion attack: dish-shaped pits (usually) between NaCl crystals, crevice corrosion under NaCl crystals, and pits within crevices under NaCl crystals. The widths of the pits found between crystals were smaller than the pits observed in droplets containing only $MgCl_2$ with the same CDD. This can be attributed to an increased IR drop (due to the presence of

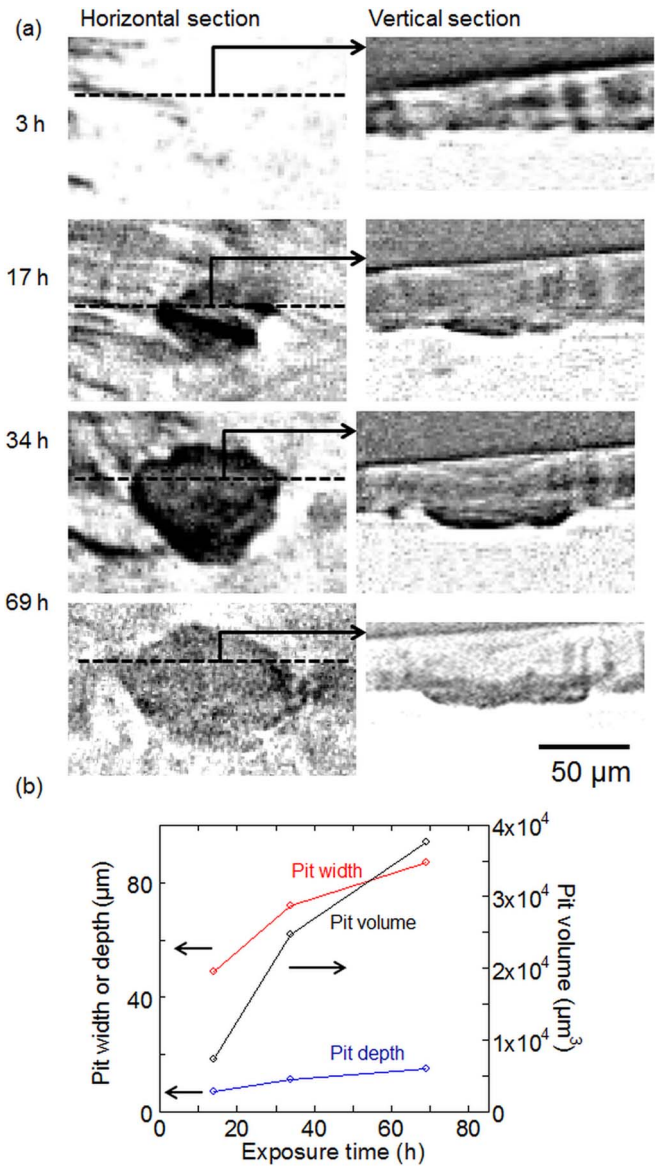

Figure 8. Horizontal and vertical sections of the tomogram of crevice-like attack (shown in Figure 4) imaged with X-ray microtomography on a 2 mm 304 pin deposited with a $1MgCl_2$:2NaCl mixed salt droplet with a CDD of 2000 µg/cm^2 following exposure at 45 ± 2% RH and 21 ± 1°C for 3 h, 17 h, 34 h and 69 h. (b) Width, depth and volume of the crevice-like attack at 17 h, 34 h and 69 h.

crystals and a lower electrolyte volume) and a lower area for oxygen reduction for the mixed salt droplets.

- In situ X-ray microtomography can be used to monitor the pit growth on metal pins. The morphologies of pits in the tomography observations are consistent with lab-based measurements.

Acknowledgments

This work was supported by EPSRC grant EP/I036397/1. LG was funded by the University of Birmingham Postgraduate Elite Scholarship. We thank Diamond Light Source for access to Beamline I12 (ee7412) that contributed to the results presented here.

ORCID

Liya Guo https://orcid.org/0000-0002-3268-9960
Angus Cook https://orcid.org/0000-0002-9173-0863
Alison J. Davenport https://orcid.org/0000-0003-0853-515X

References

1. I. S. Cole, N. S. Azmat, A. Kanta, and M. Venkatraman, *Int. Mater. Rev.*, **54**, 117 (2009).
2. ASTM, E104-02, 1951 (2012) Standard Practice for Maintaining Constant Relative Humidity by Means of Aqueous Solutions, in, West Conshohocken, PA.
3. C. Padovani, O. E. Albores-Silva, and E. A. Charles, *Corrosion*, **71**, 292 (2015).
4. C. Padovani, R. J. Winsley, N. R. Smart, P. A. H. Fennell, C. Harris, and K. Christie, *Corrosion*, **71**, 646 (2015).
5. Y. Tsutsumi, A. Nishikata, and T. Tsuru, *Corrosion Sci.*, **49**, 1394 (2007).
6. B. Maier and G. S. Frankel, *J. Electrochem. Soc.*, **157**, C302 (2010).
7. N. Mi, M. Ghahari, T. Rayment, and A. J. Davenport, *Corrosion Sci.*, **53**, 3114 (2011).
8. S. R. Street, N. Mi, A. Cook, H. B. Mohammed-Ali, L. Y. Guo, T. Rayment, and A. J. Davenport, *Faraday Discuss.*, **180**, 251 (2015).
9. Y. H. Wang, W. Wang, Y. Y. Liu, L. Zhong, and J. Wang, *Corrosion Sci.*, **53**, 2963 (2011).
10. E. Tada and G. S. Frankel, *J. Electrochem. Soc.*, **154**, C318 (2007).
11. W. Y. Lv, C. Pan, W. Su, Z. Y. Wang, S. N. Liu, and C. Wang, *Journal of Materials Engineering and Performance*, **24**, 2597 (2015).
12. S. Hastuty, A. Nishikata, and T. Tsuru, *Corrosion Sci.*, **52**, 2035 (2010).
13. ASTM, D1141-98(2008) Standard Practice for the Preparation of Substitute Ocean Water, in, ASTM International, West Conshohocken (2008).
14. S. P. Knight, M. Salagaras, A. M. Wythe, F. De Carlo, A. J. Davenport, and A. R. Trueman, *Corrosion Sci.*, **52**, 3855 (2010).
15. N. Mi, Synchrotron X-ray Studies of Atmospheric Pitting Corrosion of Stainless Steel, PhD thesis, *School of Metallurgy and Materials*, University of Birmingham (2013).
16. A. du Plessis, Stuides of atmospheric corrosion processes in AA2024, PhD thesis, *School of Metallurgy and Materials*, University of Birmingham (2014).
17. S. M. Ghahari, A. J. Davenport, T. Rayment, T. Suter, J. P. Tinnes, C. Padovani, J. A. Hammons, M. Stampanoni, F. Marone, and R. Mokso, *Corrosion Sci.*, **53**, 2684 (2011).
18. T. J. Marrow, L. Babout, A. P. Jivkov, P. Wood, D. Engelberg, N. Stevens, P. J. Withers, and R. C. Newman, *J. Nucl. Mater.*, **352**, 62 (2006).
19. F. Eckermann, T. Suter, P. J. Uggowitzer, A. Afseth, A. J. Davenport, B. J. Connolly, M. H. Larsen, F. D. Carlo, and P. Schmutz, *Corrosion Sci.*, **50**, 3455 (2008).
20. B. J. Connolly, D. A. Horner, S. J. Fox, A. J. Davenport, C. Padovani, S. Zhou, A. Turnbull, M. Preuss, N. P. Stevens, T. J. Marrow, J. Y. Buffiere, E. Boller, A. Groso, and M. Stampanoni, *Mater. Sci. Technol.*, **22**, 1076 (2006).
21. A. J. Davenport, C. Padovani, B. J. Connolly, N. P. C. Stevens, T. A. W. Beale, A. Groso, and M. Stampanoni, *Electrochem. Solid State Lett.*, **10**, C5 (2007).
22. A. J. Davenport, L. Guo, N. Mi, H. Mohammed-Ali, M. Ghahari, S. R. Street, N. J. Laycock, T. Rayment, C. Reinhard, C. Padovani, and D. Krouse, *Corrosion Engineering, Science and Technology*, **49**, 514 (2014).
23. M. Drakopoulos, T. Connolley, C. Reinhard, R. Atwood, O. Magdysyuk, N. Vo, M. Hart, L. Connor, B. Humphreys, G. Howell, S. Davies, T. Hill, G. Wilkin, U. Pedersen, A. Foster, N. De Maio, M. Basham, F. J. Yuan, and K. Wanelik, *Journal of Synchrotron Radiation*, **22**, 828 (2015).
24. J. Schindelin, I. Arganda-Carreras, E. Frise, V. Kaynig, M. Longair, T. Pietzsch, S. Preibisch, C. Rueden, S. Saalfeld, B. Schmid, J.-Y. Tinevez, D. J. White, V. Hartenstein, K. Eliceiri, P. Tomancak, and A. Cardona, *Nature Methods*, **9**, 676 (2012).
25. L. Guo, Atmospheric Localised Corrosion of Type 304 Austenitic Stainless Steels, PhD thesis, *School of Metallurgy and Materials*, University of Birmingham (2015).
26. D. J. Cziczo, J. B. Nowak, J. H. Hu, and J. P. D. Abbatt, *J. Geophys. Res.-Atmos.*, **102**, 18843 (1997).
27. Y. G. Gao, S. B. Chen, and L. E. Yu, *Atmos. Environ.*, **41**, 2019 (2007).
28. E. Schindelholz, L. K. Tsui, and R. G. Kelly, *J. Phys. Chem. A*, **118**, 167 (2014).
29. I. N. Tang, H. R. Munkelwitz, and J. G. Davis, *Journal of Aerosol Science*, **8**, 149 (1977).
30. D. D. Weis and G. E. Ewing, *Journal of Geophysical Research: Atmospheres*, **104**, 21275 (1999).
31. M. E. Wise, G. Biskos, S. T. Martin, L. M. Russell, and P. R. Buseck, *Aerosol Sci. Technol.*, **39**, 849 (2005).
32. A. Cook, C. Padovani, and A. J. Davenport, *J. Electrochem. Soc.*, **164**, C148 (2017).
33. W. Xu, Synchrotron X-ray and Electrochemical Studies of Pitting Corrosion of Iron, PhD thesis, *School of Metallurgy and Materials*, University of Birmingham (2014).
34. Z. Nagy and H. You, *J. Electroanal. Chem.*, **381**, 275 (1995).
35. Z. Y. Chen and R. G. Kelly, *J. Electrochem. Soc.*, **157**, C69 (2010).
36. M. Ghahari, D. Krouse, N. Laycock, T. Rayment, C. Padovani, M. Stampanoni, F. Marone, R. Mokso, and A. J. Davenport, *Corrosion Sci.*, **100**, 23 (2015).
37. F. King, P. Robinson, C. Watson, J. Burrow, and C. Padovani, ACSIS - A model to assess the potential for atmospheric corrosion of stainless steel ILW containers during interim storage and the operational phase of a UK geological disposal facility, in *Proc. 2013 NACE Corrosion Conf.*, p. paper 2717 (2013).
38. L. Guo, S. Zhou, L. Crocker, and A. Turnbull, *International Journal of Fatigue*, **98**, 195 (2017).